Engineering Structures 125 (2016) 455–470

Contents lists available at ScienceDirect

Engineering Structures

journal homepage: www.elsevier.com/locate/engstruct

Out-of-plane shaking table tests on URM single leaf and cavity walls

Francesco Graziotti [a,b,*], Umberto Tomassetti [a], Andrea Penna [a,b], Guido Magenes [a,b]

[a] Dept. of Civil Engineering and Architecture, University of Pavia, via Ferrata 3, 27100 Pavia, Italy
[b] European Centre for Training and Research in Earthquake Engineering, via Ferrata 1, 27100 Pavia, Italy

ARTICLE INFO

Article history:
Received 27 April 2016
Revised 16 June 2016
Accepted 8 July 2016
Available online 25 July 2016

Keywords:
Cavity walls
URM
Out-of-plane
Rocking
Shaking table test
One-way bending
Coefficient of restitution

ABSTRACT

Damage observations from recent seismic events have confirmed that the activation of out-of-plane local mechanisms is one of the major causes of structural collapse in unreinforced masonry buildings. Particularly vulnerable are cavity walls commonly used in residential building in regions such as Central and Northern Europe, Australia, New Zealand, China and several other countries. Usually, the inner leaf has a load-bearing function, carrying vertical loads transmitted by floors and roof while the outer leaf, having only aesthetic and insulation functions, is lightly loaded. The two leaves are typically connected by means of metallic ties. The high out-of-plane vulnerability, which may prevent the exploitation of the global capacity associated with the in-plane capacity of the structural walls, is mainly due to the high slenderness of the masonry leaves and the lack, or ineffectiveness, of ties between leaves. Often ties are too widely spaced and/or heavily degraded. Despite the complexity of the composite behaviour of such a construction typology, no dynamic tests on cavity walls are reported in current literature. For this reason, four out-of-plane shaking table tests were conducted on full-scale unreinforced masonry assemblies of three cavity wall panels with different tie distributions (inner calcium silicate brick wall and outer clay brick wall) and one single-leaf wall constructed using calcium silicate brick masonry. The experimental arrangement allowed the specimens to be tested under different input signals and loading conditions, inducing an out-of-plane one-way bending action in the walls. The research is aimed at understanding the seismic behaviour of cavity walls, their failure mechanisms and how they are affected by boundary conditions and degree of connection between the two leaves. The paper describes the main experimental results, including deformed shapes, damage patterns, force-displacement relationships, and the capacities in term of acceleration sustained by the specimens. Additionally, the energy dissipation involved in the mechanism has been investigated in terms of coefficient of restitution and damping ratio. All the processed data are freely available upon request (see http://www.eucentre.it/nam-project).

1. Introduction

Over the last decades, observations of damage caused by major earthquake events have shown that the structural collapse in unreinforced masonry (URM) buildings is very often associated with the activation of out-of-plane overturning mechanisms, rather than the attainment of maximum stress in structural elements: such overturning mechanisms are activated by the loss of equilibrium in masonry portions due to out-of-plane (OOP) actions. This behaviour is often associated with the lack of good connections to adjacent perpendicular walls and floors (e.g. [1–3]). Cavity wall buildings are particularly vulnerable to out-of-plane actions due to the walls being both slender and lightly loaded, which prevents the development of their full in-plane strength capacity. Cavity construction is a form of wall construction where a cavity is left between the two leaves of bricks. Sometimes insulating material is inserted in the cavity. The external leaf of a cavity wall is often a brick veneer wall without any load bearing function, whereas the internal leaf is a load-bearing wall, carrying the vertical loads transmitted by the floors and roof. It is common for the inner leaf to be constructed with different materials than the outer leaf. In several European countries an example of this solution is to have the inner wall made of calcium silicate bricks/blocks, whereas the outer wall uses clay bricks. Leaves on either side of a cavity wall are typically connected by regularly spaced metal cavity ties, which can vary in material, shape and spacing. Because of their relatively light weight, good thermal insulation properties and effective protection against driving rain, cavity walls are widely used in

* Corresponding author at: Dept. of Civil Engineering and Architecture, University of Pavia, via Ferrata 3, 27100 Pavia, Italy.
E-mail address: francesco.graziotti@unipv.it (F. Graziotti).

http://dx.doi.org/10.1016/j.engstruct.2016.07.011
0141-0296/

Central and Northern Europe countries, especially for residential constructions.

Experience on the seismic behaviour of cavity walls is quite limited, and mostly related to earthquakes which have occurred in Australia (Newcastle, 1989) and New Zealand (Christchurch sequence, 2010–2011). Dizhur and Ingham [4] noted three primary types of out-of-plane wall failures in cavity wall buildings following the Christchurch earthquakes: (i) vertical (or one-way) bending of the wall (7% of the cases), which tended to occur in longer walls or walls without side supports; (ii) two-way bending (57% of the cases), which required support of at least one vertical edge of a wall and (iii) top portion cantilever type failure with the entire top section of a wall or building façade collapsing, mainly due to a lack of top horizontal restraint.

The OOP failures may affect the entire wall (both leaves), especially in front façades or upper storey walls of many two-storey buildings, or otherwise may affect the external leaf only. This high vulnerability is mostly due to the slenderness of the masonry leaves and the lack or inefficiency of anchoring systems between leaves. The leaf connections (ties) are often too widely spaced and embedded in weak mortar, which results in the pull-out of the anchoring systems. Corrosion of ties has also been repeatedly reported as strongly affecting their effectiveness [2–5]. In addition, another primary cause of failure observed in cavity wall buildings is the lack of appropriate wall-to-diaphragm and wall-to-floor connections. The seismic OOP assessment of solid walls with top support has been already the subject of significant experimental investigations (among others [6–11]) and the theoretical modelling of such response was also carried out resorting to rigid-body idealizations. Very little experimental research, instead, has been carried on the seismic behaviour of cavity walls. In particular, no dynamic tests on cavity walls are presently available in the literature.

This paper presents experimental results which were obtained as a part of a wider research project aimed at assessing the vulnerability of URM buildings in the Groningen (the Netherlands) region, which in the last two decades has been exposed to induced seismicity [12]. Currently, very limited data are available on the seismic response of construction typologies specific to Dutch practice. The project, started in 2014, aims at investigating the performance of structural components, assemblies and systems typical of building typologies present in the Groningen area. The experimental campaign includes in situ mechanical characterization tests and laboratory tests such as characterization tests on bricks, mortar and small masonry assemblies, in-plane cyclic shear-compression and dynamic out-of-plane tests on full-scale masonry piers. Shaking table tests on full-scale masonry house specimens have also been performed at the laboratory of EUCENTRE Pavia. The experimental campaign aims to be a solid reference for the development of reliable numerical models to be used in fragility curves development and in the assessment of the seismic risk.

This paper describes out-of-plane shaking table tests on full-scale masonry assemblies. Three specimens represented different cavity wall configurations with different tie distributions, and one was a single-leaf wall specimen. The test set-up was constructed in order to induce OOP one-way bending behaviour in the specimens. The effect of vertical edge boundary conditions, reported also in earthquake damage observations (e.g. two way bending, see Fig. 1b), was deliberately not considered, as a first approach to the problem, and the horizontal double-fixed boundary conditions were designed in order to be always known in every testing phase. This allowed for a reduction of the unknowns and a simplification of the problem to the advantage of the subsequent interpretation and possible use of the data for model calibration.

Section 2 of the paper provides information on the specimen geometry and their material characterization. Section 3 provides a detailed description of the test-setup and the observed testing programme. The test results including deformed shapes, failure mechanisms, damage patterns, energy dissipation and other specific features of the observed dynamic behaviour are presented in Section 4. Part of such information is also reported in Tomassetti et al. [13].

2. Characterization of the masonry specimens

2.1. Specimen construction and geometric characterization

Under controlled laboratory conditions, professional masons built the specimens in accordance with Dutch practices common in the years 1970–1980. The specimens were composed of one single leaf wall made of Calcium Silicate (CS) bricks and three cavity wall panels with an inner CS brick wall (density 1835 kg/m^3) and an outer clay brick wall (density 1950 kg/m^3), with an 80 mm air gap. The two masonry leaves were approximately 2750 mm high, h, 1450 mm wide, w, and 102 mm thick, t. The sizes of the bricks were respectively $212 \times 102 \times 71$ for the CS bricks and $211 \times 100 \times 50$ for the clay bricks. The mortar bed-joints were nominally 10 mm thick in both walls. The specimens differed in terms of the applied vertical overburden pressure, σ_v (0.1 and

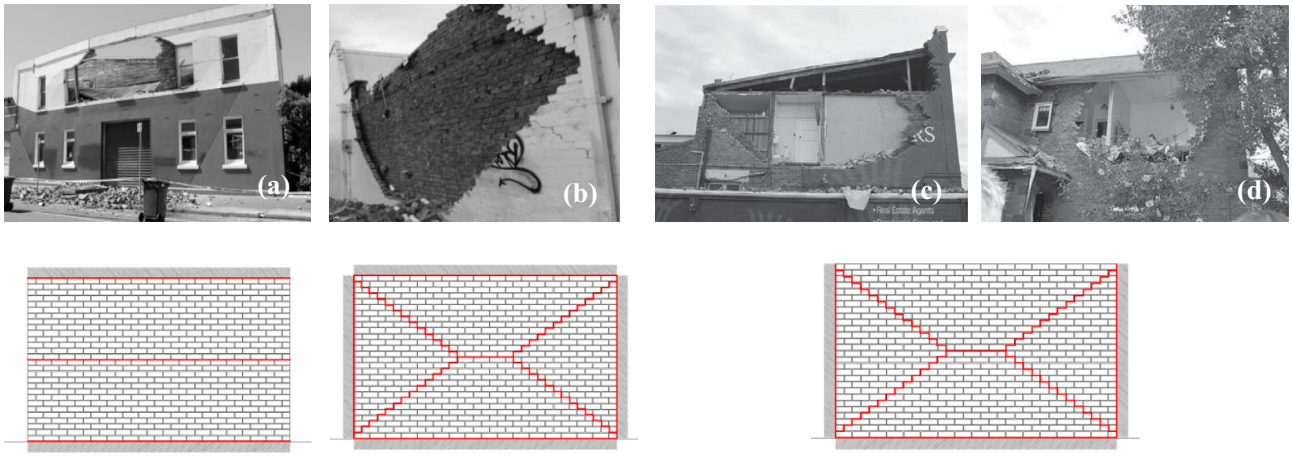

Fig. 1. One-way bending failure (a), two-way failure (b), top portion cantilever wall failure (c, d) (adapted from Dizhur et al. [2]).

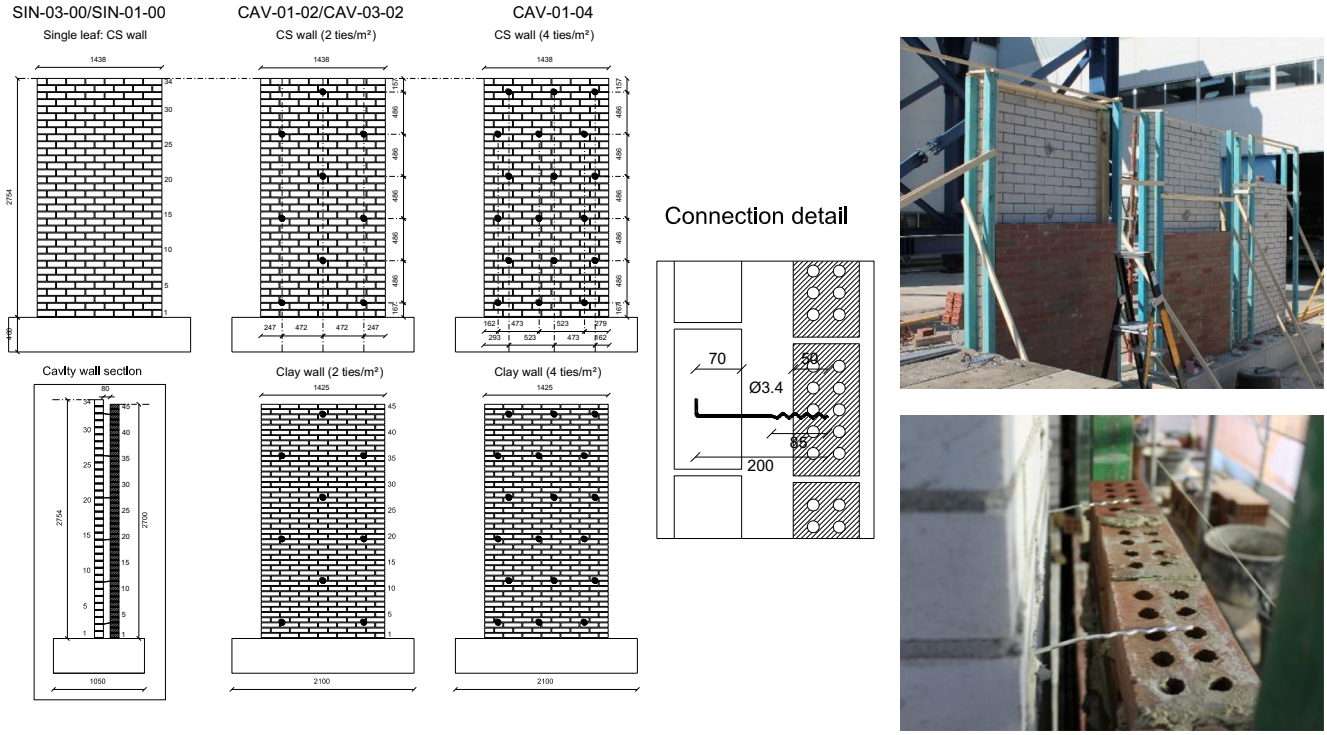

Fig. 2. Specimens geometry and construction details.

Table 1
Characteristics of test specimens.

Specimen ID	Wall type	w [mm]	t [mm]	h [mm]	σ_v [MPa]	Ties/m^2 [–]
SIN_03_00	Single CS leaf wall[a]	1438	102	2754	0.3	–
SIN_01_00	Single CS leaf wall[a]	1438	102	2754	0.1	–
CAV_01_02	CS inner wall	1438	102	2754	0.1	2
	Clay outer wall	1425	100	2700	0	
CAV_03_02	CS inner wall	1438	102	2754	0.3	2
	Clay outer wall	1425	100	2700	0	
CAV_01_04	CS inner wall	1438	102	2754	0.1	4
	Clay outer wall	1425	100	2700	0	

[a] Same specimen for both configurations.

0.3 MPa), and number of ties, which were chosen according to code prescriptions and common masonry practices (2 and 4 ties/m^2, see Fig. 2). These levels of imposed overburden pressure could be considered representative of a loadbearing wall located at the second and first storeys respectively, of a classical two storeys residential building. They are not meant to represent upper or lower bounds, but rather common values that can be often found in real buildings. L shape steel ties with a diameter of 3.1 mm and 200 mm long were inserted in the mortar bed-joints during the laying of the bricks to connect the two masonry leaves (see detail in Fig. 2). Tests on pull-out strength of this specific coupling system were performed by Messali et al. [14] at TU Delft. Those researchers found that the pull-in and pull-out strengths of the "zigzag" tie extremity embedded in clay masonry specimens, considering an overburden pressure of 0.3 MPa, resulted higher than the strengths associated with the hook extremity embedded in CS specimens and subjected to the same imposed pressure. The average pull-out and push-in strengths recorded for CS specimens were approximately 1.46 kN and −1.09 kN, respectively. Moreover, the tensile ultimate capacity of the steel anchors was approximately 4.3 kN. Table 1 identifies the specimens, their geometry, tie configuration and the applied overburden pressure.

Even if the scope of the present tests was envisaging idealized boundary conditions, the specimens could be somehow representative of a single storey vertically spanning cavity wall between two RC slabs and separating two tall windows; the floor system, usually, lies only on the inner CS wall, while the outer wall is continuous over the full height of the building. Moreover, often there is no physical connection at the diaphragm level between the floor system and the outer clay wall. A full-scale house specimen with these specific construction details has been tested on the shake table at the EUCENTRE laboratory in Pavia, and will be the subject of a future publication.

2.2. Mechanical characterization of the materials

A detailed overview of the experimental test campaign on material samples and masonry wallettes performed at the laboratory of the Department of Civil Engineering and Architecture of the University of Pavia is provided in Graziotti et al. [15]. Table 2 summarises experimental mean values, standard deviations (*St.Dev.*) and coefficients of variation (*C.o.V.*) for the investigated mechanical parameters, namely compressive strength (f_m), Young's Modulus in compression (E) and the flexural tensile strength (f_w) of masonry perpendicular to bedjoints. The first two parameters were determined on masonry specimens according to EN 1052-1 [16], while the last one by means of the bond wrench tests as per EN 1052-5 [17]. Moreover, the mortar's compressive (f_c) and flexural strength (f_t) values were determined according to EN 1015-11 [18] and shown in Table 2 (shaded cells).

It can be appreciated how the CS masonry is characterized by a lower compression strength but a higher tensile (bond) strength compared to the clay brick masonry. In general, the mechanical characteristics of clay masonry resulted to have a dispersion higher than the one of CS masonry. This may be possibly related to the higher scatter in the properties of the components used for the clay

Table 2
Results of characterization tests on mortar and masonry specimens.

	Calcium silicate					Clay				
	f_c	f_t	f_m	f_w	E	f_c	f_t	f_m	f_w	E
Mean [MPa]	6.77	2.77	6.20	0.238	3256	6.09	2.03	11.32	0.158	5760
St.Dev. [MPa]	0.88	0.25	0.41	0.039	641	1.16	0.47	1.31	0.092	1613
C.o.V. [%]	13.0	9.0	7.0	16.3	20.0	19.0	23.0	12.0	58.2	28.0

brick masonry and to the lower bond developed between mortar and clay bricks.

3. Test set-up and dynamic loading sequence

3.1. Test set-up

The test set-up was installed on a uni-directional shake table and oriented to excite the specimens in OOP one-way bending. Fig. 3 shows some pictures of the test setup. Frame A, designed to be rigid, ensured that the dynamic input motion was transferred from the table to the top of the wall with negligible amplification. The specimens were anchored through the foundation to the shake table by means of steel bolts. The CS wall (representing the load-bearing wall in a real structure) was vertically loaded to the desired initial axial stress value through a steel beam pulled down by means of two steel rods in series with two springs (as shown in Fig. 3d). The connection between frame A and the beam on top of the specimen consisted of a pair of steel braces with mechanical hinges at one end (Fig. 3c).

The braces were rigidly connected to the specimen top beam by means of steel plates in order to avoid any relative rotation. The hinge system allowed for the uplift of the wall whilst simultaneously transferring the horizontal dynamic input of the shake table to the top of the specimen. The resulting static configuration of the inner wall was that of double fixed boundary conditions. The restraint at the top of the inner wall was provided by a set of L-shaped steel profiles and mortar was used to fill the gap to the top row of bricks (see Fig. 3c). The bottom section of the wall specimen lay on a mortar bed-joint resting on the specimen foundation, as in usual practice. A spring system was used to provide the axial force (see Fig. 3d) on the CS wall and ensure that the increase in axial force at collapse (when the wall height is maximum), computed considering a rigid body failure mechanism, was less than 5% higher than the initial static force. The designed spring stiffness, experimentally tested, was 164.7 N/mm for those used to provide 0.3 MPa of axial stress and 53.5 N/mm for those providing 0.1 MPa stress. This solution guaranteed a double fixed condition with almost constant overburden axial stress in the inner CS wall during all the testing phases. This condition was not necessarily representative of a wall in a real building subjected to ground motions. In that case, the axial force was likely changing during the motion due to a general redistribution of axial forces in the building as well as to the partial restrained uplift of the wall induced by the floor. The aim of the test was to support the calibration of numerical models, for this reason the boundary conditions were designed to be always known and idealized. The outer clay brick leaf did not have any restraint or load applied at the top, being supported on the foundation and connected to the CS leaf by the metal ties.

A safety system was designed in order to prevent the complete out-of-plane collapse of the specimens and potential damage of equipment and instrumentation. This system consisted of two adjustable steel frames supporting transparent polycarbonate panels, which were modified to allow the installation of wire displacement transducers to the wall specimens. The safety system was able to accommodate a maximum displacement at mid-height of about 100 mm.

3.2. Instrumentation and data acquisition

Fig. 4 provides a side view of the test setup, which also shows the reference system (positive towards the clay walls side) and the position of instruments that were used for the shake table testing. Accelerometers were installed in order to record the applied acceleration histories at the specimen foundation, on the top beam and on the right and left frames. Additional accelerometers were installed on the wall panels in order to monitor their mid-height response. Wire potentiometers (WP), attached to the two side frames A and B (both considered rigid), were installed up the height of the specimens (on the vertical axis of symmetry) in order to record the horizontal displacement of the walls relative to the shake table. Vertical displacement transducers were also installed on the spring system to monitor the spring shortening and in turn

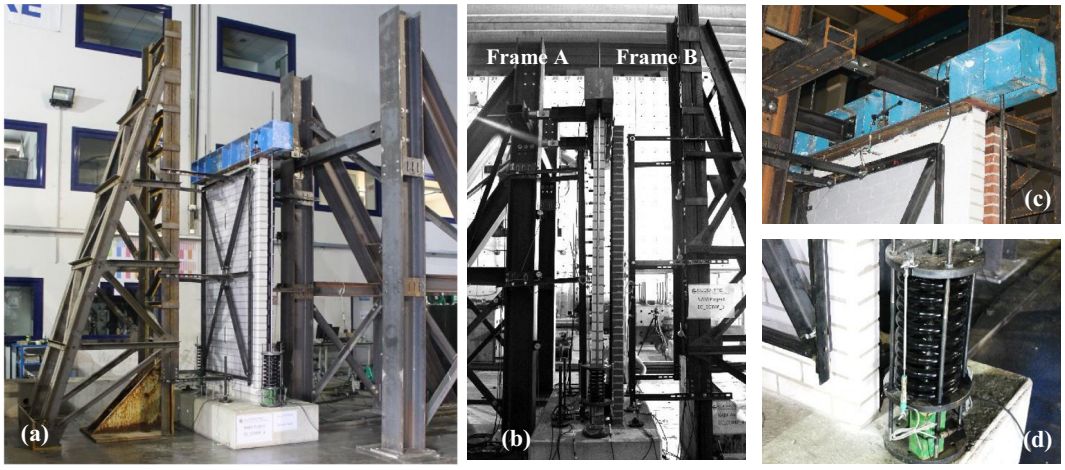

Fig. 3. Specimens geometry and details: general view (a, b), top boundary condition (c) and spring system (d).

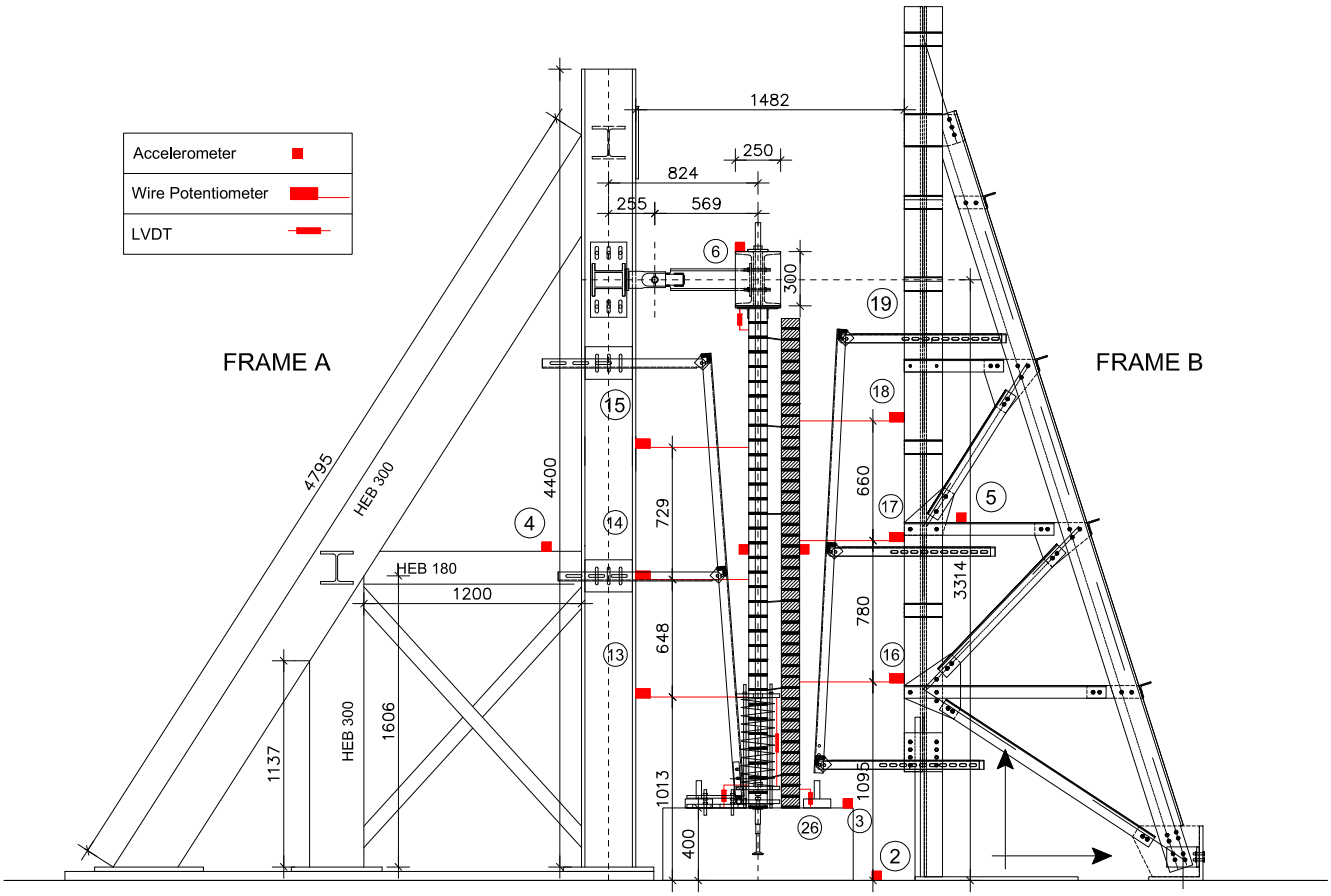

Fig. 4. Side view of the test set-up and instrumentation.

the applied overburden force during all the testing phases. Additional vertical transducers were installed on the 2nd and 33th brick layers of the inner wall in order to detect significant rotations with respect to the 1st and 34th brick layers, respectively (the number of layers is indicated in Fig. 2).

Table 3 indicates the position in height of the instruments with respect to the top of the concrete foundation.

3.3. Dynamic input motion

Three acceleration time histories were employed in these dynamic tests. Gr-1 was supplied by the seismic hazard and risk assessment team involved in the project [12] as representative of an expected ground motion in the region of Groningen. The Gr-2 input was instead a first floor accelerogram obtained by means of the TREMURI program [19] using a model of a typical Dutch terraced house subjected to the aforementioned Gr-1 record along its flexible direction. A further input signal is represented by the 2 Hz Ricker Wave Acceleration input (RWA), which consists of a particular acceleration pulse (also known as Mexican hat wavelet). As a reference, Figs. 5 and 6 show the 100% theoretical acceleration time-histories of the experimental inputs and their response spectra, respectively.

Table 3
Vertical position of the instruments installed on the specimens.

Instrument	SIN-03-00 SIN-01-00 [mm]	CAV-01-02 [mm]	CAV-03-02 [mm]	CAV-01-04 [mm]
1/4 WP CS	612	612	695	693
1/2 WP CS	1340	1341	1503	1503
3/4 WP CS	1900	1900	2151	2151
1/4 WP CI	–	695	610	610
1/2 WP CI	–	1475	1355	1342
3/4 WP CI	–	2135	1955	1990
4/4 WP CI	–	–	2650	2650
1/2 Acc. CS	1260	1341	1341	1503
1/2 Acc. CI	–	1295	1355	1355

3.4. Testing programme

Initially, the specimens were subjected to low amplitude random excitations in order to identify their undamaged dynamic properties. The second testing phase consisted of an incremental dynamic testing procedure with the Gr-1 accelerograms, which could be considered a realistic excitation for a wall located at the ground floor of a building. Therefore, a series of Gr-1 acceleration table motions scaled to increasing amplitude were performed. A second incremental dynamic testing sequence was performed with the Gr-2 accelerograms, representing a possible dynamic excitation for a wall located at the building first floor, up until collapse of the specimen. A pulse excitation phase (adopting the RWA input) has been run between Gr-1 and Gr-2 in order to obtain samples of simplified wall response. These are ideal for the calibration of numerical models and studying the damping. Repetitions of tests with inverted directions (polarity) were performed in order to understand if, and how, the excitation direction affects the specimens' responses. The specimen/experiment listed as SIN_03_00 in Table 1 is the wall previously tested as SIN_01_00, where the test set-up was modified by substituting the springs in order to increase the axial stress acting on the inner leaf from 0.1 to 0.3 MPa. Tables 4 and 5 present the applied dynamic testing sequence, corresponding to the single-leaf and the cavity speci-

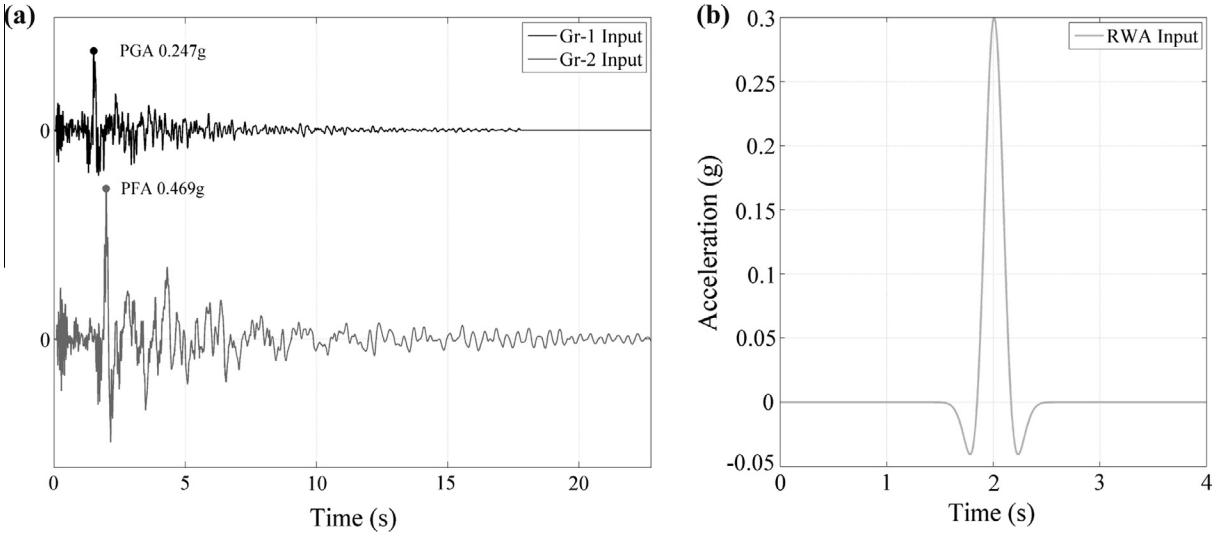

Fig. 5. Gr-1, Gr-2 (a) and RWA (b) acceleration time histories.

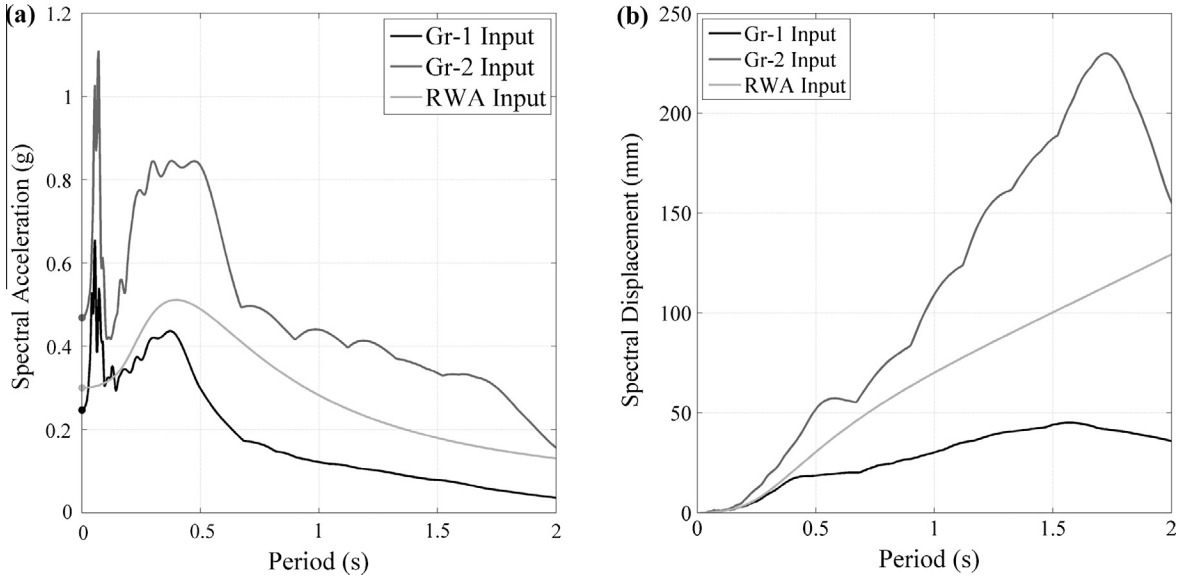

Fig. 6. Comparison of acceleration (a) and displacement (b) response spectra (5% damping) for the adopted input signals.

Table 4
Single-leaf specimen testing sequence.

SIN-03-00 σ_v = 0.3 MPa				SIN-01-00 σ_v = 0.1 MPa			
Test #	Input	PGA [g]	Peak R. [mm]	Test #	Input	PGA [g]	Peak R. [mm]
0.1	WN	–	–	0.2	WN	–	–
1.1	Gr_1	+0.04	+0.06	3.1	Gr_1	+0.08	−0.35
1.2	Gr_1	+0.09	+0.11	3.2	Gr_1	+0.17	−0.73
1.3	Gr_1	+0.16	+0.40	3.3	Gr_1	+0.21	−0.92
1.4	Gr_1	+0.20	+0.57	3.4	Gr_1	+0.34	−1.28
1.5	Gr_1	+0.32	+0.92	3.5	Gr_1	+0.41	+1.94
1.6	Gr_1	+0.42	+1.22	3.6	Gr_1	+0.51	−7.42
1.7	Gr_1	+0.52	+1.40	3.7	Gr_1	+0.60	−14.42
1.8	Gr_1	+0.74	+1.70	3.8	Gr_1	+0.73	−16.60
1.9	Gr_1	+0.96	+4.93	4.1	RWA	−0.26	−0.38
2.1	RWA	−1.11	−1.97	4.2	RWA	−0.48	−1.88
2.2	**RWA**	**−1.63**	**−9.63**	**4.3**	**RWA**	**−0.72**	**−16.05**
2.3	RWA	−1.05	−2.68	**4.4**	**RWA**	**−0.96**	**−52.98**
2.4	**RWA**	**−1.88**	**−14.1**	5.1	Gr_2	+0.44	+2.87
				5.2	Gr_2	+0.64	−9.86
				5.3	Gr_2	+0.85	**–fail**

mens respectively, and specifying the test number, the dynamic input typology, the peak acceleration, PGA, recorded on the specimen foundation during the test and the peak horizontal mid-height CS wall displacement response recorded by correspondent wire potentiometer. The overall chronological testing sequences are provided in Tables 4 and 5, in order to better understand the state of degradation of the specimens at the beginning of each considered test. The tests best suited for the estimation of the energy dissipation (Section 4.6) are large amplitude RWA pulses (highlighted in bold characters). The shaded sections of the table identify different testing phases.

4. Test results

The test set-up proved to be effective in allowing the specimens to be tested with the desired boundary conditions and inducing a pure OOP one-way bending action in the walls. Fig. 7a shows the comparison between the top and bottom response spectra computed from the recorded shake table acceleration histories and

Table 5
Cavity wall specimen testing sequence.

CAV-01-02 σ_v = 0.1 MPa, 2 ties/m^2				CAV-03-02 σ_v = 0.3 MPa, 2 ties/m^2				CAV-01-04 σ_v = 0.1 MPa, 4 ties/m^2			
Test#	Input	PGA *[g]*	Peak R. *[mm]*	Test#	Input	PGA *[g]*	Peak R. *[mm]*	Test#	Input	PGA *[g]*	Peak R. *[mm]*
0.1	WN	-	-	0.1	WN	-	-	0.1	WN	-	-
1.1	Gr_1	+0.04	+0.00	1.1	Gr_1	+0.08	-0.18	1.1	Gr_1	+0.03	+0,05
1.2	Gr_1	+0.09	+0.12	1.2	Gr_1	+0.12	-0.24	1.2	Gr_1	+0.09	-0,08
1.3	Gr_1	+0.12	+0.19	1.3	Gr_1	+0.17	+0.15	1.4	Gr_1	+0.13	-0.17
1.4	Gr_1	+0.17	+0.31	1.4	Gr_1	+0.21	+0.28	1.5	Gr_1	+0.17	-0.26
1.5	Gr_1	+0.21	+0.36	1.5	Gr_1	-0.08	-0.04	1.6	Gr_1	+0.21	+0.36
1.6	Gr_1	-0.08	-0.15	1.6	Gr_1	-0.12	+0.12	2.1	RWA	+0.31	+0.33
1.7	Gr_1	-0.13	+0.20	1.7	Gr_1	-0.16	-0.11	2.2	RWA	-0.34	-0.50
1.8	Gr_1	-0.17	-0.40	1.8	Gr_1	-0.20	-0.14	3.1	Gr_2	+0.30	+0.60
1.9	Gr_1	-0.23	-0.54	2.1	RWA	+0.29	+0.65	3.2	Gr_2	+0.44	+1.47
2.1	RWA	-0.22	-0.34	2.2	RWA	-0.29	-0.41	3.3	Gr_2	+0.63	-2.89
2.2	RWA	-0.32	-0.65	3.1	Gr_2	+0.30	+0.64	3.4	Gr_2	+0.73	-45.5
3.1	Gr_2	+0.33	-0.74	3.2	Gr_2	+0.44	+0.99	4.1	RWA	-0.30	-4.66
3.2	Gr_2	+0.50	+2.45	3.3	Gr_2	+0.63	+1.70	4.2	RWA	+0.31	+2.25
3.3	Gr_2	+0.60	-10.6	3.4	Gr_2	+0.75	-2.88	0.2	WN	-	-
4.1	Gr_1	+0.61	-42.4	4.1	RWA	+0.50	+1.90	**4.5**	**RWA**	**+0.50**	**-28.8**
5.1	RWA	-0.32	-3.20	4.2	RWA	-0.52	-2.00	**4.6**	**RWA**	**-0.53**	**-45.3**
5.2	**RWA**	**-0.49**	**+40.42**	5.1	Gr_2	+0.93	-6.12	5.1	Gr_2	+0.44	-32,9
6.1	Gr_2	+0.68	**-fail**	5.2	Gr_2	+1.11	**-fail**	5.2	Gr_2	+0.62	**-fail**
								5.3	Gr_2	-0.49	-
								5.4	Gr_2	-0.68	**+fail**

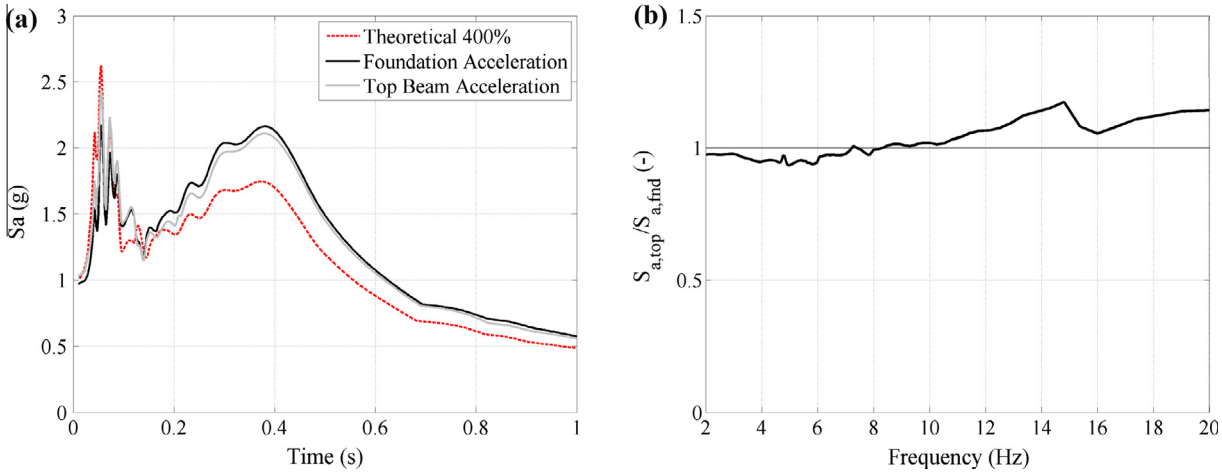

Fig. 7. Spectral accelerations comparison (a) and spectral acceleration ratio (b) between specimen top and bottom locations for the specimen SIN-03-00 (test 1.9).

the theoretical, or target, response spectra for a relevant Gr-1 test (e.g. SIN-03-00, test 1.9, input scaled to 400%). It is possible to observe some discrepancy between the target and the recorded acceleration spectrum due to the dynamic interaction between the test setup and the shaking table. The consequent distortion in the recorded response spectra is higher for tests with larger PGAs (as the one presented in Fig. 7a) and considerably smaller for test of lower intensity. A slightly undershoot of low period spectral accelerations is detectable while a more consistent overshoot (amplification) is seen for the higher periods. Fig. 7b shows the top and bottom acceleration spectrum ratio considering just the frequency range relevant for the dynamic behaviour of the specimens. A slight amplification (not exceeding 15%) is detectable corresponding to the steel frame fundamental frequency of vibration (≈15 Hz). Notice that all the accelerations (nominal and recorded) during each testing phases are stored and available for processing.

4.1. Dynamic identification

As already mentioned, all specimens were excited by means of a random signal (0.05*g* PGA), in order to detect the fundamental frequency of vibration of the undamaged wall. Analysing the mid-height acceleration response of both walls, significant amplifications corresponding to the natural frequency of vibration of the wall were detected. Table 6 lists the natural frequencies of vibration for each specimen obtained from the random test.

4.2. Deformed shapes

The deformed shapes have been obtained from the horizontal displacement recorded by the wire potentiometers at the time of maximum displacement of the CS wall at mid-height. As expected, deformed shapes change significantly according to the ground motion intensity level and specimen damage. Fig. 8a shows the

Table 6
Specimen dynamic identification.

Specimen	CS wall		Clay wall	
	Frequency [Hz]	Period [s]	Frequency [Hz]	Period [s]
SIN_03_00	18.75	0.053	–	–
SIN_01_00	14.27	0.070	–	–
CAV_01_02	17.23	0.058	20.08	0.049
CAV_03_02	25.00	0.040	20.68	0.048
CAV_01_04	19.24	0.052	19.13	0.052
CAV_01_04[a]	13.08	0.076	7.11	0.141

[a] Performed after test 4.2.

specimens' deformed shapes from the Gr1 tests (intensity 100% PGA 0.247*g*) where the peak acceleration direction is towards the clay wall side (positive direction).

The deformed shape of the single-leaf wall is approximately similar to that of a double fixed beam, with the response peaks located at 1/2 of the wall height for both the SIN-03-00 and SIN-01-00 configurations.

In cavity wall specimens, the CS wall deformed shapes were qualitatively similar to those recorded for the single-leaf walls. The clay wall, instead, due to the different stiffness and top boundary conditions, tended to displace differently exhibiting almost a cantilever deformed shape. Because of this, the relative horizontal displacement between the two walls is higher at the top, as shown by the CAV_01_02 and CAV_03_02 specimens. A progressive deterioration of the bond of the tie anchoring system, which resulted in the recording of a few millimetres of differential displacement between the two leaves, has been detected in these testing phases, even for low intensity levels of shaking. Such a phenomenon is less evident for the CAV_01_04 specimen where the density of ties is higher and consequently the relative displacement of the walls resulted to be lower.

Fig. 8b shows the deformed shapes associated with all the specimens for different RWA input tests where the peak acceleration direction is towards the CS wall side (negative direction). As the acceleration input and the horizontal displacement increase, the deformed shapes change significantly. The specimens exhibited rocking behaviour with the formation of cracks at bottom, top and around mid-height sections. For cavity specimens, the differential displacement between the two leaves became progressively negligible with respect to the amplitude of the two walls mid-height displacement.

No top cracks in cavity specimens were detected in the clay wall, which was unrestrained at the top. The two quasi-rigid bodies above and below the mid-height crack sections rotated around the cracked sections, using them as pivot points and displacing simultaneously. It is possible to notice differences in the response of the panels: the CAV_03_02 specimen shows a considerably lower mid-height displacement when subjected to inputs with similar PGAs while the CAV_01_02 wall exhibited a peak mid-height response in the opposite direction of the acceleration pulse.

4.3. Damage pattern and failure mechanisms

All the specimens exhibited rocking behaviour with the formation of horizontal cracks at the bottom, top and around mid-height sections of the walls. For cavity wall specimens, cracks at the wall top were detected only on the CS walls, with the tops of the clay walls being unrestrained. Fig. 9 identifies the location of cracks for the single-leaf specimen and for cavity wall specimens in both the CS walls and clay walls (in terms of layer number). The tie grid is also shown to better understand the position of the cracks with respect to the anchoring system between the two walls.

The single-leaf specimen, which exhibited rocking only when subjected to 0.1 MPa of vertical overburden pressure (SIN-01-00), showed a mid-height crack at 0.575·*h* (between the 19th and the 20th brick layer), where *h* is the nominal wall height, taken as the total panel height minus the height of one brick (due to the last brick layer being clamped by the steel L-shape profiles). The observed mechanism agrees well with the formulation proposed in literature for the estimation of the intermediate hinge height considering the wall tensile strength [20], which yielded a value 0.557·*h* according to the following equation:

$$\frac{h_1}{h} = 1 + \frac{\eta + t - \sqrt{(2 + t + 2\eta)(t + \eta)}}{2 + \eta} = 0.557 \tag{1}$$

where $\eta = O/W$ is the ratio between vertical overburden force and the wall self-weight and $t = f_w/(W/(t \cdot w))$ is the non-dimensional masonry tensile strength. The parameter t significantly influences the position of the mid-height hinge: the higher the tensile strength, the lower its position. Moreover, it is important to underline that Eq. (1) has been proposed for the case when the vertical overburden force is applied at the wall mid-thickness; however, during the experimental test there is a migration of the resultant

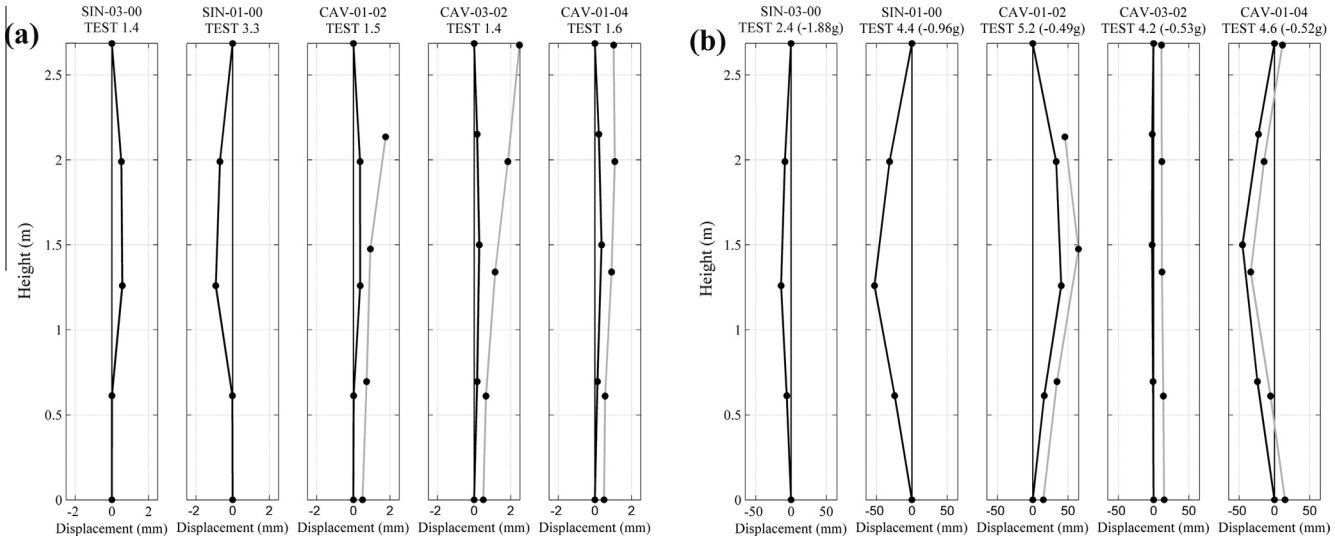

Fig. 8. Deformed shapes for Gr1 (a) and RWA (b) input: CS wall black line, clay wall grey line.

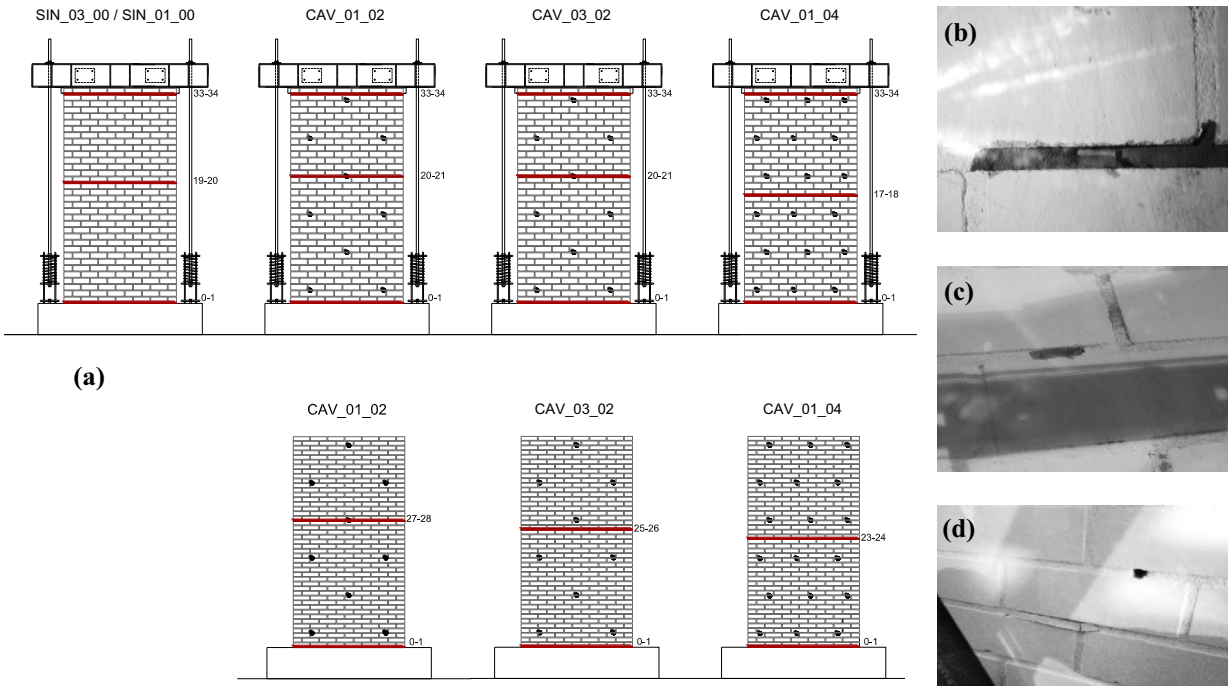

Fig. 9. Specimens crack pattern (top CS wall, bottom clay wall) (a) and pictures of damage detected on the CS wall for the CAV-01-02 (b), CAV-03-02 (c) and CAV-01-04 (d).

overburden force (O) towards the thickness edge (hinge location) during the rocking behaviour (see Fig. 10).

For cavity wall specimens, instead, it can be observed that for the two specimens with a tie density of 2 ties/m^2 (CAV_01_02 and CAV_03_02) the horizontal mid-height cracks are at a height of approximately 0.6h, which is the height of the tie connection between the two walls. The CAV_01_04 specimen/test (which had 4 ties/m^2) showed instead mid-height cracks at exactly 0.5h. Further cracks (not reported in the figure) developed only after the impact with the safety system and they cannot be considered part of the failure mechanism. Damage at the mortar bed-joints in the CS walls was detected at some of the locations corresponding to the position of the ties (see Fig. 9b–d). This was caused by the relative positioning of the ties along the thickness of the leaf (the hook was always closer to the outer face of the CS leaf); the pull-out capacity in the positive direction (e.g. clay wall pulling the CS wall) was higher than in negative direction (e.g. clay wall pushing the CS wall) as found by [14].

The observed behaviour, as largely suggested in literature [8,20,21], can be described by the dynamic response of an assembly of rigid bodies. Fig. 10, shows a rigid body schematic representation of the experimental test performed for the single-leaf wall and for the cavity specimens. The upper portion is represented by the last brick layer clamped by the L steel profiles and free to move vertically due to the mechanical hinge on the left arms extremity (see Fig. 3c).

Looking at Fig. 10, it may be observed that, with the incoming uplift of the wall, the overburden resultant axial force migrates towards the thickness edge of the CS wall (passing through the pivot point C). The wall, indeed, displacing horizontally switches

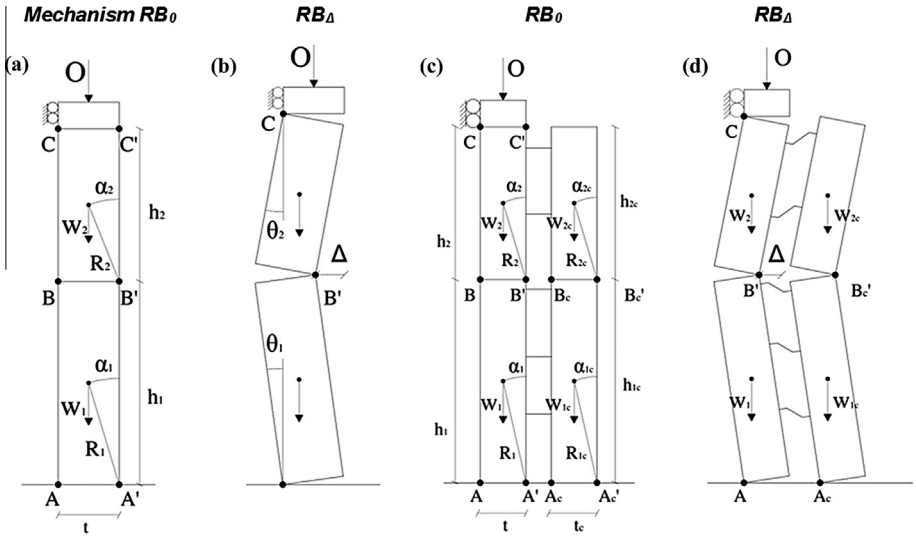

Fig. 10. Rigid body (RB) mechanisms: static and dynamic conditions for single-leaf (a, b) and cavity wall (c, d) specimens.

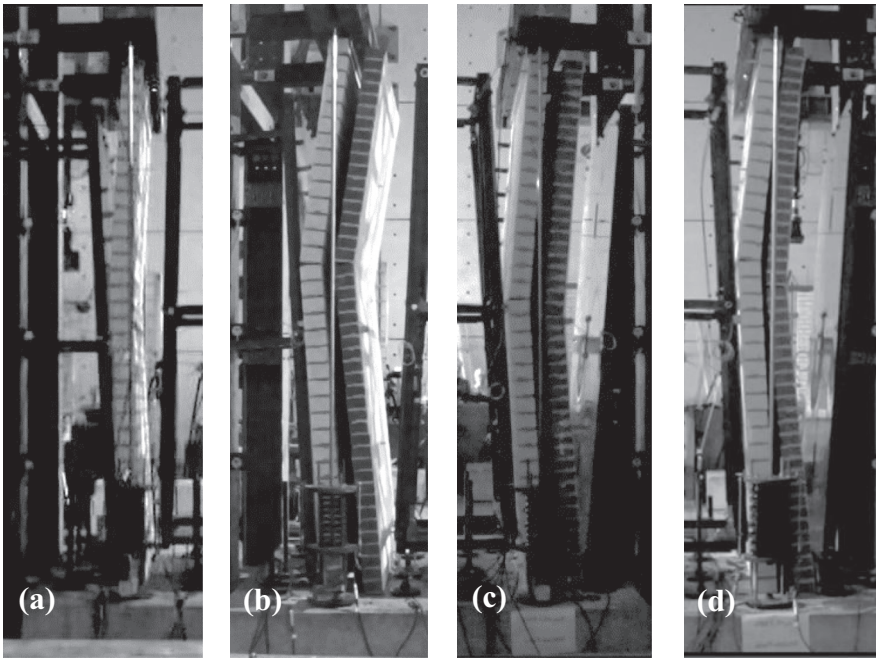

Fig. 11. Snapshots of the specimen failures: SIN-01-00 (a), CAV-01-02 (b), CAV-01-04 (c) and CAV-03-02 (d).

from an ideal RB mechanism with the axial force applied at the mid-thickness (RB_0) to a RB mechanism where the force is applied at the thickness edge (RB_Δ). The horizontal weight multiplier that triggers those mechanisms and the associated instability displacements (when the wall resisting force drops to zero) is slightly different. Moreover, for a better understanding of the dynamic behaviour and the failure mechanisms involved, Fig. 11 presents frames of the video at the moment of the specimens collapses. In particular, it is possible to appreciate the deformed shapes during the test and in the instants before the impact against the restraining system. All the cavity specimens collapsed under the Gr-2 earthquake towards the CS wall. It is believed that this fact, which is different from what observed in many real earthquakes (where often the outer leaf collapses outwards and the inner leaf remains standing) is probably the result of a combination of the following factors: (a) the input acceleration, characterized by short duration and non-symmetric pulses (a "directional effect" in the input), and (b) the mechanical and geometrical characteristics of the ties, whose anchor strength is lower in the push direction and which also may easily buckle in compression. Especially this latter factor (b) leads the outer leaf to sway more easily towards the stiffer inner leaf, since the ties oppose a lower reaction when failing in compression, while it is more effectively restrained by the ties and the inner leaf when trying to sway away from it, in the outward direction. CAV-01-02 (Fig. 11b) and CAV-01-04 (Fig. 11c) specimens exhibited rocking behaviour in several tests before the failure whereas the CAV-03-02 (Fig. 11d) exhibited a rocking behaviour only right before collapsing.

All the cavity specimens collapsed in horizontally-coupled one-way rocking behaviour and exhibited damage due to failure in compression of the anchoring of the steel ties into the mortar bed-joints of the CS walls. Although the ties had negligible flexural stiffness, their axial stiffness ensured a sufficient coupling of the horizontal displacement of the two leaves (i.e. limiting the differential displacement and maintaining the gap) up to near-collapse, even for the specimens with only 2 ties/m^2, producing a one-way rocking failure mechanism in the cavity components. This is extremely important as it allows for the analysis of the OOP seismic behaviour of these cavity walls with simplified single-degree of freedom (SDOF) models, as proposed by several studies for solid walls [8,20,21]. This simplification may not necessarily be generalized to cavity walls with geometry and boundary conditions which are very different from those tested here. The present tests show that, for this specific cavity wall configuration (e.g. material strengths, geometry, ties positioning, un-degraded materials, input motions) the weak direction seems to be the inward one due to the failure in compression of the ties. This behaviour may not be necessarily representative of the behaviour of the entire building stock, if different ties or masonry leaves are present.

4.4. Specimen F-Δ relationships

For the dynamic simulation of the OOP response of walls, the definition of a reliable capacity curve F-Δ (where F is the total horizontal force while Δ defines the horizontal displacement of the mid-height hinge) is crucial. For single-leaf vertical spanning strip wall (VSSW), this relationship was successfully modelled by a tri-linear curve by several researcher that provided mean parameters necessary to build such configuration [8,22–24]. Ferreira et al. [25] proposed instead, a four branch model. This section presents the experimental F-Δ curves for the single-leaf specimen and for the cavity specimens. Another experimental research project aimed at understanding the static F-Δ relationship of cavity walls with New Zealand detailing has been carried out by Walsh et al. [26]. Within the presented experimental campaign, TU Delft performed OOP static tests on components with typical Dutch detailing (as the one herein presented). Fig. 12 shows the comparison between the experimental dynamic F-Δ curve and the RB bi-linear curves associated with static mechanisms RB_0 and RB_Δ (see Fig. 10).

The experimental force has been obtained by multiplying the absolute acceleration of the centre of mass of the two bodies by the related masses while the displacement is the one relative to the mid-height hinge location. The two centre of mass accelerations were computed using the acceleration recorded by the mid-height accelerometer and assuming a triangular distribution of the relative acceleration along the wall height, with the maximum

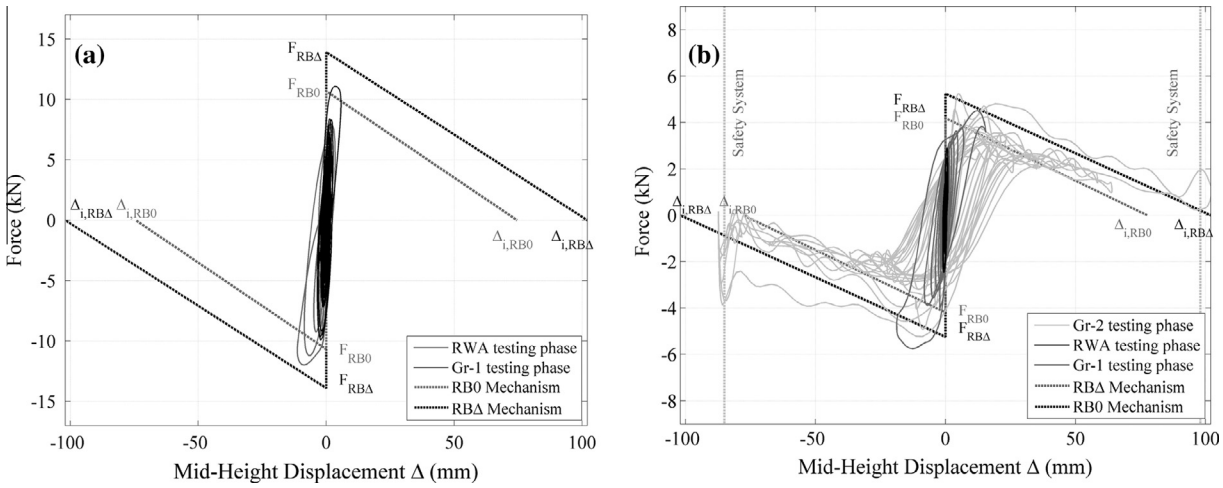

Fig. 12. Single-leaf specimen F-Δ relationships: SIN-03-00 (a) and SIN-01-00 (b).

Table 7
Rigid-body force-displacement bi-linear parameters.

	Mechanism RB_0	Mechanism RB_Δ
F_{RB}	$F_{RB0} = \frac{2}{h_1}(W+O)t + \frac{1}{h-h_1}Ot$	$F_{RB\Delta} = \frac{2}{h_1}(W+O)t + \frac{2}{h-h_1}Ot$
$\Delta_{i,RB}$	$\Delta_{i,RB0} = \frac{\left[\frac{W+O}{h_1}+\frac{O}{2(h-h_1)}\right]}{\left[\frac{W+O}{h_1}+\frac{O}{(h-h_1)}\right]}t$	$\Delta_{i,RB\Delta} = t$

value at the mid-height hinge location (e.g. considering the two bodies as rigid). The RB bilinear static relationships have been built according to the two idealisations considering the corresponding instability displacements. Table 7 summarises the parameters necessary to build the bi-linear relationships (e.g. the static capacity curve) for the rigid body mechanisms shown in Fig. 10.

Fig. 13 shows the comparison between the experimental *F-Δ* curve and the RB bi-linear curves for the two mechanisms shown in Fig. 10 (right) for the cavity wall specimens. The RB force has been computed by the raw sum of the RB forces associated with the two independent mechanisms for the two walls (CS and Clay walls). The vertical grey lines (dotted) represent maximum horizontal displacements allowed by the safety system in different phases of the test. For the RB_Δ mechanism the only maximum force is plotted. Regarding the experimental *F-Δ* curve, the displacement at mid-height of the CS wall is shown.

The energy dissipation, in good part associated with the area enclosed by the hysteresis loops, is significantly higher than the single-leaf specimen cases. It is also interesting to notice that the specimen force capacity is not far from the simple sum of the forces associated to the RB mechanisms of the two walls considered independently. The capacity shown by CAV-01-02 and CAV-01-04 is comparable even if the latter was able to resist more significant runs of excitation.

4.5. Specimens' acceleration capacity

This section presents the results of the experimental incremental tests (Gr-1 and Gr-2 inputs) in terms of mid-height horizontal displacement recorded by the wire potentiometer on the CS walls and PGAs (see Fig. 14). The experimental work confirmed that the single-leaf wall capacity and the cavity wall capacity as well is strongly influenced by the overburden pressure acting. It can be observed also that in general the presence of an unloaded veneer clay wall reduce the specimens' capacity, resulting as an additional mass on the system with a very little contribution to the specimen's resistance. All the tested cavity wall specimens, in fact, exhibited lower capacities compared to the single-leaf specimen loaded at the same initial vertical force value (collapsed under Gr2-input with a PGA of 0.85*g*).

The CAV-03-02 specimen (σ_v = 0.3 MPa) collapsed when subjected to an acceleration time history with a PGA of 1.11*g*, 65% higher than the maximum applied to CAV-01-02 specimen (σ_v = 0.1 MPa).

The number of ties connecting the two walls does appear to influence the cavity wall response, with the CAV-01-04 (4 ties/m^2) specimen exhibiting an almost 10% higher capacity than the CAV-01-02 specimen (2 ties/m^2). This was associated with a general capacity to resist a larger number of excitations. The CAV-01-04 specimen resisted a maximum PGA of 0.73*g*; after this test the specimen was subjected to a further series of RWA inputs collapsing only 6 runs later under a lower peak acceleration (0.62*g* Gr-2 input). As already reported, it is interesting to note that all the specimens collapsed in the negative direction.

4.6. Energy dissipation

Another crucial parameter for the simulation of the OOP dynamic behaviour of rocking systems and for the development of reliable SDOF systems is the energy dissipation involved in such a behaviour. The rocking behaviour herein described has been extensively investigated in the past. Housner [27], under the criteria of no sliding, no bouncing effect and energy dissipation concentrated at the instant of the impact, defined a SDOF equation of motion for the simulation of the dynamic response of rigid blocks. Sorrentino et al. [20], under similar criteria and assuming both supports moving simultaneously, derived a SDOF equation of motion for vertical spanning strip walls (VSSW) (as the one herein tested, e.g. SIN-03-00 and SIN-01-00) displacing as an assembly of two rigid bodies. DeJong and Dimitrakopoulos [21] and Restrepo [28] extended the solution to include equivalent SDOF systems governing the dynamic behaviour of complex multi-block systems responding in rocking. All of the aforementioned studies described the rocking phenomena as function of the equivalent rotation of the system and simulated the energy dissipation involved in the mechanism by means of the coefficient of restitution.

4.6.1. The classical rocking theory

Housner [28] introduced a measure of the energy dissipation as the reduction of kinetic energy between the instants before and

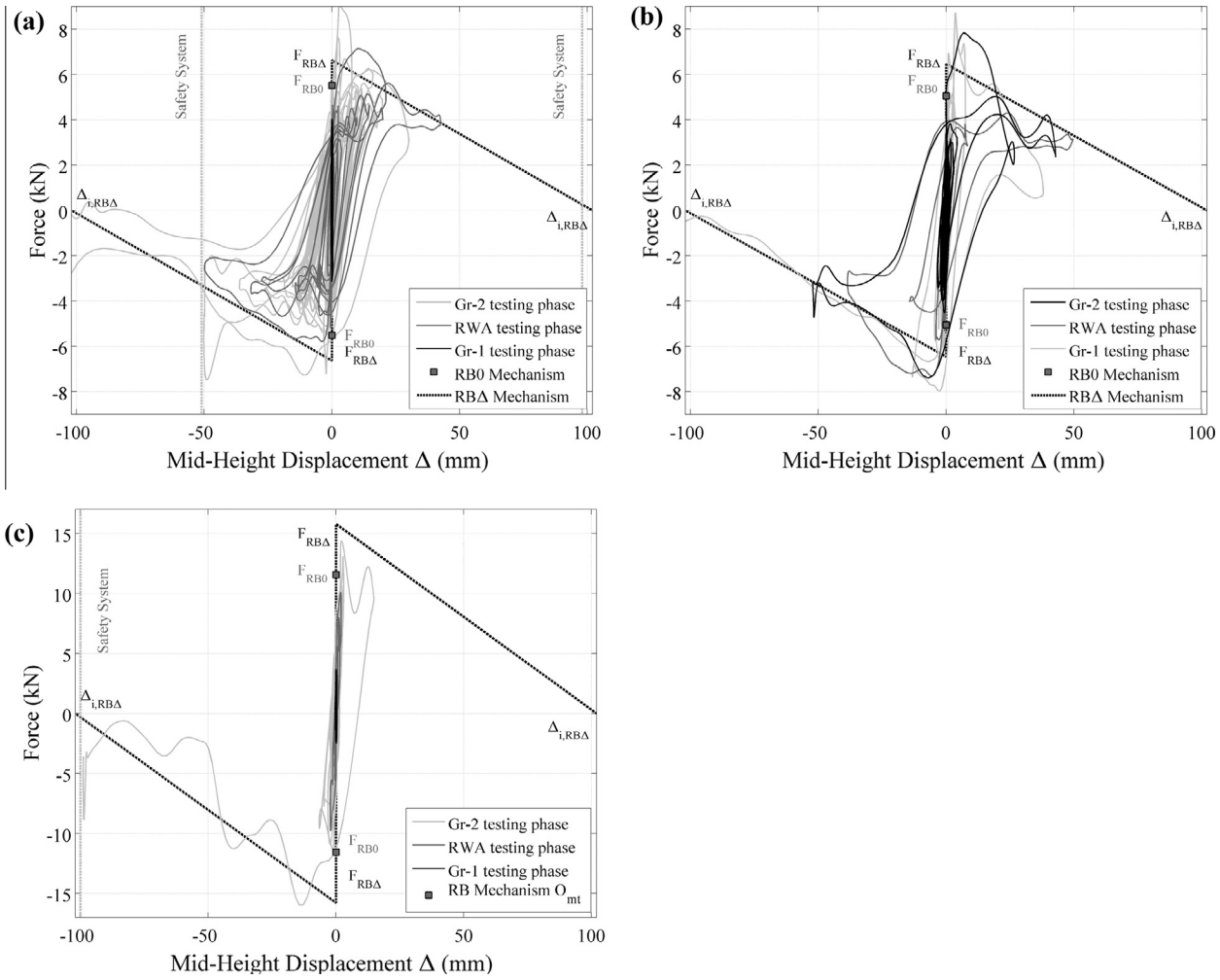

Fig. 13. Cavity wall specimen F-Δ relationships: CAV-01-02 (a), CAV-01-04 (b) and CAV-03-02 (c).

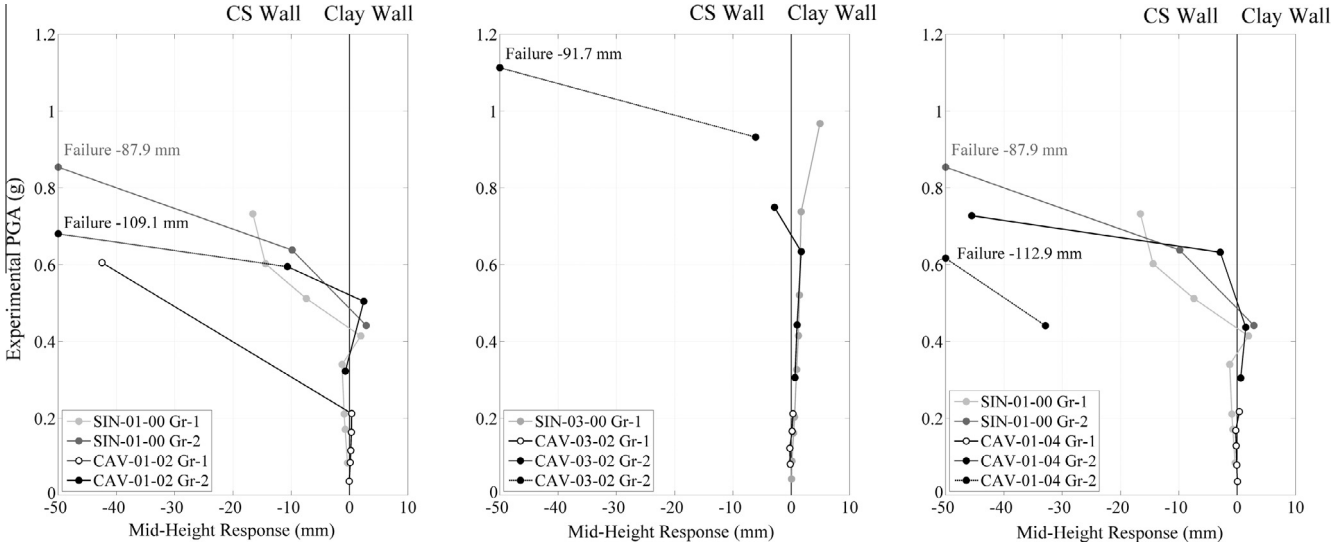

Fig. 14. Experimental PGA vs peak horizontal mid-height displacement.

after the impact. Aslam et al. [29] defined the restitution coefficient as the direct ratio between angular velocities after and before the impact. Assuming an infinitesimal impact duration and hence instant velocity variation, in analogy with Housner's formulation for the single rigid block, it is possible to derive for a VSSW system a theoretical coefficient of restitution as a ratio e_{an} between the

angular velocities after ($\dot{\theta}_{n+1}$) and before ($\dot{\theta}_n$) the impact. This coefficient is derived assuming the conservation of angular momentum around the lower rotation hinge by equating the angular momentum after and before the impact. Eq. (2) [20] provides an estimation of the velocity reduction for a VSSW knowing the geometric parameters of the wall.

$$e_{an} = \frac{\dot{\theta}_{n+1}}{\dot{\theta}_n} = \frac{m_1 R_1^2 + I_{G,1} - I_{G,2}\frac{\tan\alpha_2}{\tan\alpha_1} - 2m_1 R_1^2 \sin^2\alpha_1 + m_2 R_1^2\left[2 + \frac{\sin\alpha_1\cos\alpha_1}{\tan\alpha_2} - \sin^2\alpha_1\left(4 + \frac{\tan\alpha_2}{\tan\alpha_1}\right)\right]}{m_1 R_1^2 + I_{G,1} - I_{G,2}\frac{\tan\alpha_2}{\tan\alpha_1} + m_2 R_1^2\left[2 + \sin\alpha_1\cos\alpha_1\left(\frac{1}{\tan\alpha_2} + \tan\alpha_2\right)\right]} \quad (2)$$

where $I_{G,1}$ and $I_{G,2}$ are the polar moment of inertia around the two blocks centre of mass, while m_1 and m_2 are the two block masses and all the other parameters are defined according to Fig. 10. The coefficient of restitution, depends on the α_1 parameter: the squatter the wall (higher α_1 or lower slenderness), the higher is the energy dissipation (lower e_{an}) in analogy with the single block case. Moreover, Sorrentino et al. [20] showed also that e_{an} is much more sensitive to α_1 than to α_2 (Fig. 10a) and that the migration of the mid-height hinge towards the mid-height of the wall increases the energy dissipation.

4.6.2. Experimental computation of the coefficient of restitution

The theoretical values of the coefficients of restitution have been compared to those observed analysing the response of the specimens subjected to RWA impulses. The responses of the specimens are characterized by a significant damped free vibration phase, which provided precious information on the damping acting on the specimens. An experimental coefficient of restitution, according to the Aslam et al. [29] formulation and taking in account the assumption presented above, can be computed from angular velocity histories by manipulating and deriving the recorded mid-height displacement histories. The identification of the position of the pivot point and the subsequent kinematic transformation of the recorded displacement histories into rotation histories is extremely important in the analysis of the rocking mechanism. In reality, the two bodies do in fact have finite stiffness and the mortar bed-joint represents a flexible interface [30,31]; this leads to an inwards shift of the hinge with respect to the perfect RB mechanism. The rotation and the hinge position are hence functions of the oscillation amplitude as well as the instability rotation. Considering the high slenderness ($\lambda \approx 26$) of the tested specimens, the model assumed for the definition of the kinematic quantities involved is the RB one. The rotation history is obtained by dividing the horizontal displacement history recorded by the height of the wire potentiometer. Fig. 15a and b plot the rotation and angular velocity time histories normalised with respect to the instability rotation (A) considering a mechanism with the vertical load applied on the wall thickness edge for the SIN-01-00 specimen (test 4.4) and the CAV-01-04 specimen (test 4.6). It is possible to appreciate, as largely known for rocking systems, the dependence of the frequency of the response on the oscillation amplitude. The CAV-03-02 specimen did not show significant free vibration oscillations in the RWA tests and therefore did not allow a straightforward computation of the energy dissipation.

Therefore, a first experimental estimation of the coefficient of restitution is obtained from peak angular velocity responses of the lower body. In order to avoid inconsistencies in its computation (e.g. $e > 1$) due to the slight asymmetry of the response observed in some tests, it was computed with response peaks of the same side of motion, thus assuming that the coefficient of restitution is constant for two consecutive peaks. It has been computed according to Eq. (3):

$$e_{exp,v} = \sqrt{\frac{\dot{\theta}_{1,n+2}}{\dot{\theta}_{1,n}}} \quad (3)$$

Sorrentino et al. [20], equating the ratio between potential and kinetic energies, expressed the coefficient of restitution as a function of the peak amplitude of rotation before and after the impact. Also in this case, to avoid inconsistencies, two consecutive peaks in the same direction of motion have been considered, as was done for angular velocities. The equation is the following:

$$e_{exp,r} = \sqrt[4]{\frac{(m_1+2m_2)\left(\cos A_1^{n+2} - \cos\alpha_1\right) + m_2\frac{\sin\alpha_1}{\sin\alpha_2}\left(\cos A_2^{n+2} - \cos\alpha_2\right)}{m_1 + m_2\left[\cos^2 A_1^{n+2} + \sin^2 A_1^{n+2}\left(2 + \frac{\tan A_2^{n+2}}{\tan A_1^{n+2}}\right)^2\right] + \frac{1}{R_1^2}\left(I_{G,1} + \frac{\sin^2\alpha_1\cos^2 A_1^{n+2}}{\sin^2\alpha_2\cos^2 A_2^{n+2}} I_{G,2}\right)} \cdot \frac{(m_1+2m_2)(\cos A_1^{n} - \cos\alpha_1) + m_2\frac{\sin\alpha_1}{\sin\alpha_2}(\cos A_2^{n} - \cos\alpha_2)}{m_1 + m_2\left[\cos^2 A_1^{n} + \sin^2 A_1^{n}\left(2 + \frac{\tan A_2^{n}}{\tan A_1^{n}}\right)^2\right] + \frac{1}{R_1^2}\left(I_{G,1} + \frac{\sin^2\alpha_1\cos^2 A_1^{n}}{\sin^2\alpha_2\cos^2 A_2^{n}} I_{G,2}\right)}} \quad (4)$$

where $A_1^n = \alpha_1 - |\theta_{1,n}|$, $A_2^n = \alpha_2 - \frac{\tan\alpha_2}{\tan\alpha_1}|\theta_{1,n}|$, $A_1^{n+2} = \alpha_1 - |\theta_{1,n+2}|$ and $A_2^{n+2} = \alpha_2 - \frac{\tan\alpha_2}{\tan\alpha_1}|\theta_{1,n+2}|$ while α_1 and α_2 are geometric parameters shown in Fig. 10 and $\theta_{1,n}$ is the n-th peak rotation of the lower body. Eq. (4) leads to identical results compared with the methodology proposed by the classic analytical rocking theory [27]. Costa et al. [30] and Sorrentino et al. [32] directly used the latter formulation to compute the experimental coefficient of restitution for two different experimental campaigns on cantilever rocking masonry walls.

Fig. 16a shows a comparison between e values computed from peak angular velocities (Eq. (3)) and from peak rotations (Eq. (4))

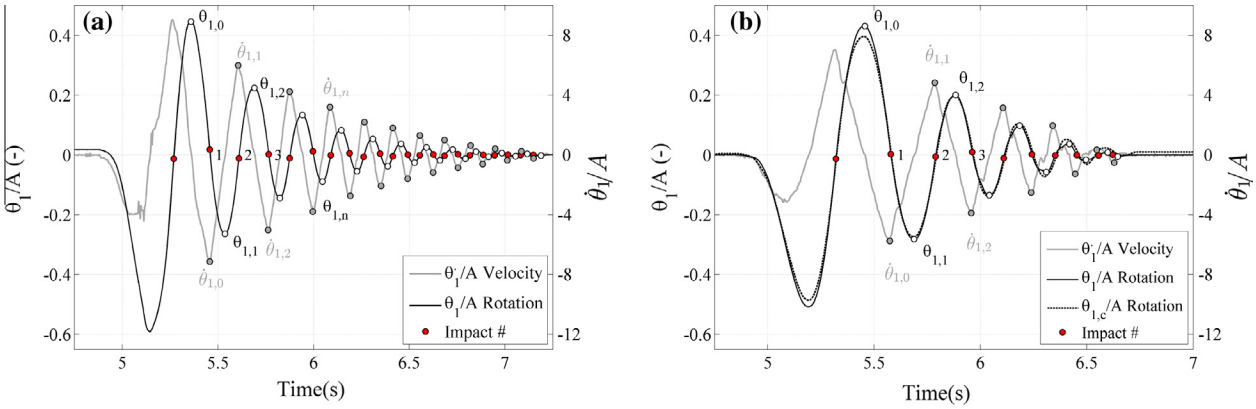

Fig. 15. Rotation and angular velocity time histories: SIN-01-00 test 4.4 (a) and CAV-01-04 test 4.6 (b).

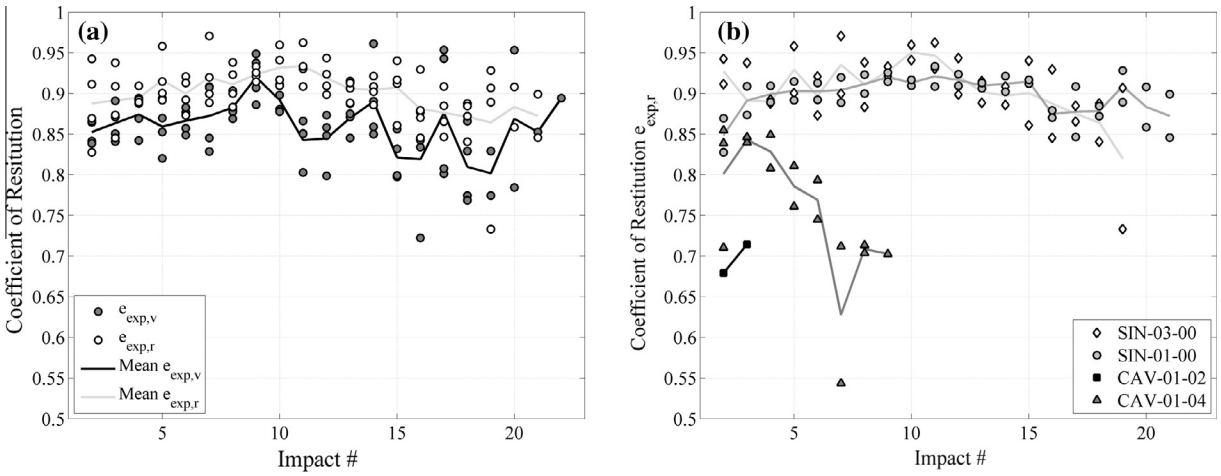

Fig. 16. Comparison between different coefficients of restitution for all the specimens (a) and comparison between coefficients of restitution $e_{exp,r}$ for different specimens (b).

Table 8
Comparison of experimental and analytical coefficient of restitution.

Specimen	e_{an}	Test	Mean $e_{exp,r}$	St. Dev. $e_{exp,r}$	Mean $e_{exp,v}$	St. Dev. $e_{exp,v}$
SIN_03_00	0.991	2.2	0.906	0.061	0.872	0.047
		2.4	0.902	0.038	0.852	0.070
SIN_01_00	0.991	4.3	0.906	0.027	0.878	0.039
		4.4	0.891	0.026	0.841	0.045
CAV_01_02	0.991	5.2	0.697	0.036	0.615	0.087
CAV_01_04	0.989	4.5	0.749	0.138	0.742	0.105
		4.6	0.785	0.084	0.713	0.203

for the single-leaf specimen (SIN-01-00 and SIN-03-00 configurations). The e_{exp} values of two consecutive impacts, computed as previously described, are assigned to the first of the two impacts. $e_{exp,v}$ provided slightly lower and more scattered values compared to $e_{exp,r}$. The former can be influenced by the resolution of the monitoring devices for small levels of rotation, while the latter has been demonstrated to successfully simulate the energy losses in simplified SDOF model. For these reasons all the results have been proposed by means of $e_{exp,r}$ [30]. The coefficients of restitution of the cavity wall specimens have been computed according to the CS inner wall crack patterns, geometry and rotation histories, taking into account the final goal of developing a reliable SDOF system that is able to simulate the OOP dynamic behaviour of cavity walls.

The $e_{exp,r}$ associated with cavity walls specimens (Fig. 16b) are much lower, due to the energy dissipated by the tie system and due to interaction between the two walls which will not move perfectly in phase, causing a significant damping effect on the system. This phenomenon is much more evident in the CAV-01-02 specimen where the number of ties is limited to 2 ties/m^2 and consequently the number of impacts detected.

Table 8 summarises the mean and standard deviation for coefficients of restitution computed for each run. No appreciable difference can be detected in the e values with the variation of the superimposed vertical load, while a slight reduction due to the specimen mortar bed joints damage at the hinge location can be detected. The ratio $e_{exp,r}/e_{an}$ for the single-leaf specimen is equal to 0.91, very close to the 0.9 value proposed by Sorrentino [24]. As expected, it is also lower than 0.95 proposed by Sorrentino et al. [32] for cantilever walls responding in rocking. Derakhshan et al. [23] recently showed that simplified models assuming a coefficient of restitution between 0.78 and 0.83 successfully simulated the dynamic response of specimens [8,9,11] squatter than the ones tested in this work.

4.6.3. Experimental computation of the damping ratio

Some authors simulated this mechanism dynamics considering the horizontal displacement correspondent to the wall mid-height hinge as the unique kinematic quantity. In these cases energy

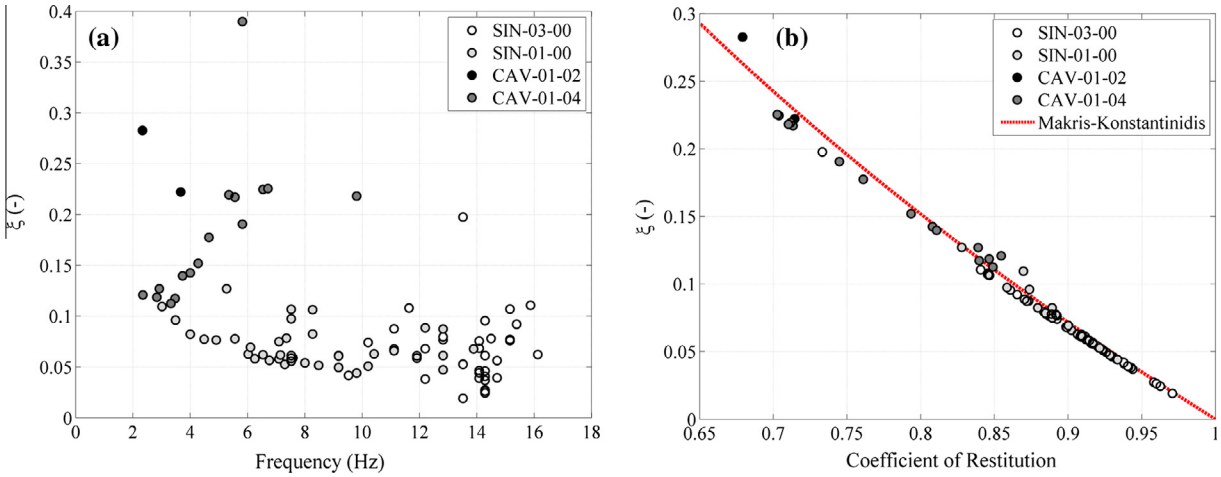

Fig. 17. Damping ratio vs frequency values (a) and coefficient of restitution vs damping ratio relationship (b).

dissipation has been modelled as a velocity dependent acting force through a constant, variable (cycle to cycle) [33] or stiffness proportional damping ratio [34]. Doherty [8] provided an estimation of the equivalent viscous damping (EVD) ratio ξ associated with the cyclic energy loss through the decay of the oscillation amplitude in a series of free vibration tests. The damping ratio was hence determined according to Eq. (5):

$$\xi = \ln(\theta_{n+2}/\theta_n)/2\pi \quad (5)$$

observing a lower bound value equal to 6%. As shown in Fig. 17a, the single-leaf specimen exhibits damping ratio values between 5 and 10%, whereas cavity specimens show values considerably higher than 10%. The change in the frequency response in the single-leaf specimen due to the different superimposed vertical load (from SIN-03-00 to SIN-01-00) is also detectable. In particular, the CAV-01-04 response appears linearly dependent on the frequency of the system, and hence on the oscillation amplitude. More tests will need to confirm this trend. Fig. 17b plots the relationship between the coefficient of restitution (computed according to Eq. (4)) and the damping ratio (computed through the logarithmic decay), for all the specimens tested. It confirms that the empirical relation between e and ξ, proposed by Makris and Konstantinidis [35] agrees well with the experimental data. Such empirical relation is presented by Eq. (6).

$$\xi = -0.68 \ln(e) \quad (6)$$

5. Conclusions

This paper presented the results of an OOP shaking table test campaign on cavity wall and single-leaf components. All the recorded signals (accelerations, displacements, videos) can be requested online (http://www.eucentre.it/nam-project). The presented work was part of an extensive experimental campaign aiming at assessing the seismic vulnerability of Dutch URM buildings. All the test specimens (single-leaf and cavity) collapsed in one-way vertical bending/rocking behaviour, exhibiting the classical top, bottom and mid-height hinges. Although the ties had negligible flexural stiffness in addition to poor mechanical characteristics of the CS wall mortar, the connections ensured a horizontally-coupled response in the cavity components and guaranteed compatibility between the two leaves' horizontal displacements, even for the specimens containing only 2 ties/m^2. This allows the analysis of the OOP seismic behaviour of cavity walls by simplified SDOF models, as previously proposed for single walls [8,20,21]. All the tested cavity wall specimens showed lower capacities when compared to the single-leaf specimen loaded with the same axial force. Damage due to failure of the bed joints caused by steel ties compression have been detected in all the cavity wall specimens. The experimental work confirmed that the specimen capacity is strongly influenced by the vertical stress acting on the walls, also for cavity walls.

The number of ties connecting the two walls does affect the cavity wall response. The CAV-01-04 (4 ties/m^2) specimen has shown almost 10% higher capacity than the CAV-01-02 specimen (2 ties/m^2) and the capability to resist a larger number of excitations. The CAV-01-04 specimen resisted, without collapse, a maximum peak acceleration of 0.73g, after this test the specimen was subjected to a further series of RWA inputs collapsing only 6 runs later under a lower peak acceleration (0.62g Gr-2 input).

The paper investigated also the force-displacement relationship and the dynamic energy dissipation involved in the mechanism. Regarding the F- Δ relationship, it is interesting to underline that the cavity components showed capacities that can be modelled starting from the sum of RB mechanisms of the two walls considered independently. The energy dissipation has been estimated assuming two damping models: the impulsive dynamics with the coefficient of restitution and the classical dynamics theory with the damping ratio. The former has been assessed around 0.90 for the single-leaf specimen with a ratio between theoretical and experimental value of 91%, close to the value of 90% obtained by Sorrentino [24]. Cavity components, due to the two walls dynamic interaction exhibited much lower values of the coefficient of restitution, i.e. 0.7 for CAV-01-02 and 0.77 for CAV-01-04, respectively. For what concerns the equivalent viscous damping ratio, values from 5 to 10% have been observed for the single-leaf specimen and much larger ones for cavity wall components (up to 30%).

Acknowledgements

This paper describes an activity that is part of the "Study of the vulnerability of masonry buildings in Groningen" project at the EUCENTRE, undertaken within the framework of the research program for hazard and risk of induced seismicity in Groningen sponsored by the Nederlandse Aardolie Maatschappij BV. The authors would like to thank all the parties involved in this project, namely EUCENTRE and University of Pavia (DICAr) laboratories that performed the tests, NAM, Arup and TU Delft. The authors are also grateful to H. Crowley and J. Bommer for defining the seismic input for the out-of-plane shaking table tests, which used the Groningen field hazard and disaggregation results provided by S. Bourne. The useful advices of professors R. Pinho, L. Sorrentino and M.C. Griffith are gratefully acknowledged. Thanks go also to M.J. Fox, I.E. Senaldi, A. Rossi and M. Mandirola for the practical support.

References

[1] Giuffrè A. A mechanical model for statics and dynamics of historical masonry buildings. In: Protection of the architectural heritage against earthquakes. Wien: Springer-Verlag; 1996. p. 71–152.
[2] Dizhur D, Ingham J, Moon L, Griffith M, Schultz A, Senaldi I, et al. Performance of masonry buildings and churches in the 22 February 2011 Christchurch earthquake. Bull NZ Soc Earthquake Eng 2011;44(4):279–96.
[3] Ingham J, Griffith M. Performance of unreinforced masonry buildings during the 2010 Darfield (Christchurch, NZ) earthquake. Aust J Struct Eng 2011;11(3):207–24.
[4] Giaretton M, Dizhur D, Da Porto F, Ingham J. Construction details and observed earthquake performance of unreinforced clay brick masonry cavity-walls. Structures 2016;6:159–69.
[5] Griffith MC. Performance of Unreinforced masonry buildings during the Newcastle Earthquake, Australia. University of Adelaide. Report no. R86; 1991.
[6] ABK. Methodology for Mitigation of seismic hazards in existing unreinforced masonry buildings: the methodology. A joint venture of Agbabian Associates, SB Barnes and Associates, and Kariotis and Associates (ABK). Topical report 08, c/o Agbabian Associates, El Segundo, California; 1984.
[7] Baggio C, Masiani R. Dynamic behaviour of historical masonry. In: Proc 9th int brick/block masonry conf, Berlin, Germany.
[8] Doherty KT. An investigation of the weak links in the seismic load path of unreinforced masonry buildings PhD thesis. Australia: University of Adelaide; 2000.
[9] Simsir CC, Aschheim MA, Abrams DP. Out-of-plane dynamic response of unreinforced masonry bearing walls attached to flexible diaphragms. In: Proc 13th world conf on earthquake engineering, Vancouver, BC, Canada.
[10] Meisl C, Elwood KJ, Ventura CE. Shake table tests on the out-of-plane response of unreinforced masonry walls. Can J Civ Eng 2007;34(11):1381–92.
[11] Penner O, Elwood KJ. Out-of-plane dynamic stability of unreinforced masonry walls in one-way bending: shake table testing. Earthquake Spectra 2016. http://dx.doi.org/10.1193/011415EQS009M [in press].
[12] NAM. Hazard and risk assessment for induced seismicity groningen. Study 1 hazard assessment; 2015. Update 1st May 2015. Available from at: <http://feitenencijfers.namplatform.nl/download/rapportdialog/e2db3b7a-1719-40cb-9002-35f9fcbd1ffd>.
[13] Tomassetti U, Graziotti F, Penna A, Magenes G. Out-of-plane shaking table test on URM cavity walls. In: Proc 16th int brick/block masonry conference, Padua, Italy.
[14] Messali F, Esposito R, Maragna M. Pull-out strength of wall ties. Report, TU Delft, NL; 2016.
[15] Graziotti F, Rossi A, Mandirola M, Penna A, Magenes G. Experimental characterization of calcium-silicate brick masonry for seismic assessment. In: Proc 16th international brick/block masonry conference, Padua, Italy.

[16] EN 1052-1. Methods of test for masonry – Part 1: determination of compressive strength. CEN/TC. European Standard; 1998.
[17] EN 1052-5. Methods of test for masonry – Part 5: determination of bond strength by the bond wrench method. CEN/TC. European Standard; 1998.
[18] EN 1015-11. Methods of test for mortar for masonry – Part 11: determination of flexural and compressive strength of hardened mortar. CEN/TC. European Standard; 1999.
[19] Lagomarsino S, Penna A, Galasco A, Cattari S. TREMURI program: an equivalent frame model for the nonlinear seismic analysis of masonry buildings. Eng Struct 2013;56:1787–99.
[20] Sorrentino L, Masiani R, Griffith MC. The vertical spanning strip wall as a coupled rocking rigid body assembly. Struct Eng Mech 2008;29:433–53.
[21] DeJong MJ, Dimitrakopoulos EG. Dynamically equivalent rocking structures. Earthquake Eng Struct Dynam 2014;43(10):1543–63.
[22] Derakhshan H, Dizhur DY, Griffith MC, Ingham JM. Seismic assessment of out-of-plane loaded unreinforced masonry walls in multi-storey buildings. Bull NZ Soc Earthquake Eng 2014;47(2):119–38.
[23] Derakhshan H, Griffith MC, Ingham JM. Seismic out-of-plane seismic response of vertically spanning URM walls connected to flexible diaphragms. Earthquake Eng Struct Dynam 2015;45(4):563–80.
[24] Sorrentino L. Dinamica di muri sollecitati fuori del piano come sistemi di corpi rigidi PhD thesis. Italy: Sapienza University of Rome; 2003 [in Italian].
[25] Ferreira TM, Costa AA, Vicente R, Varum H. A simplified four-branch model for the analytical study of the out-of-plane performance of regular stone URM walls. Eng Struct 2015;83:140–53.
[26] Walsh K, Dizhur D, Shafaei J, Derakhshan H, Ingham JM. In situ out-of-plane testing of unreinforced masonry cavity walls in as-build and improved conditions. Structures 2015;3:187–9.
[27] Housner GW. The behavior of inverted pendulum structures during earthquakes. Bull Seismol Soc Am 1963;53(2):403–17.
[28] Restrepo Vélez LF. Seismic risk of unreinforced masonry buildings PhD thesis. Italy: ROSE School, University of Pavia; 2004.
[29] Aslam M, Godden W, Scalise D. Rocking and overturning response of rigid bodies to earthquake motions. Report University of California, Berkeley, LBL-7539 UC-11; 1978.
[30] Costa AA, Arêde A, Penna A, Costa A. Free rocking response of a regular stone masonry wall with equivalent block approach: experimental and analytical evaluation. Earthquake Eng Struct Dynam 2013;42(15):2297–319.
[31] Psycharis I, Jennings P. Rocking of slender rigid bodies allowed to uplift. Earthquake Eng Struct Dynam 1983;11(1):57–76.
[32] Sorrentino L, Shawa OA, Decanini LD. The relevance of energy damping in unreinforced masonry rocking mechanisms. Experimental and analytic investigations. Bull Earthq Eng 2011;9(5):1617–42.
[33] Lam NTK, Griffith M, Wilson J, Doherty K. Time-history analysis of URM walls in out-of-plane flexure. Eng Struct 2003;25(6):743–54.
[34] Tomassetti U, Graziotti F, Penna A, Magenes G. A single-degree of freedom model for the simulation of the out-of-plane response of unreinforced masonry walls. In: Proc 16th Italian conf on earthquake engineering, L'Aquila, Italy.
[35] Makris N, Konstantinidis D. The rocking spectrum and the limitations of practical design methodologies. Earthquake Eng Struct Dynam 2003;32(2):265–89.